Interface reflection of spherical acoustic waves in the first- and second-order rational parabolic approximations and their artifacts

Maarten V. de Hoop[a)]
Koninklijke/Shell Exploratie en Produktie Laboratorium, Volmerlaan 6, 2288 GD Rijswijk ZH, The Netherlands

Adrianus T. de Hoop[b)]
Laboratory of Electromagnetic Research, Faculty of Electrical Engineering, Delft University of Technology, P.O. Box 5031, 2600 GA Delft, The Netherlands

(Received 15 June 1991; revised 10 August 1992; accepted 8 September 1992)

The accuracy of the first- and second-order rational parabolic approximations of the "vertical" slowness and the nature of the artifacts associated with them in the space-time solutions to the acoustic wave equations in a fluid medium are investigated. In particular, the reflection of an impulsive, point-source generated, spherical wave against the boundary with a medium with a higher wave speed is analyzed. From the space-time Green's functions in the relevant two-media configuration, evaluated with the aid of the modified Cagniard method, it is found that, instead of generating the real, physical head wave, the approximations generate artificial head-wavelike arrivals. The analysis makes explicit in which regions of space and in which time interval the artifacts show up and of what nature they are. Numerical results are presented.

PACS numbers: 43.20.Dk, 43.20.Px, 43.20.Bi, 43.30.Cq

INTRODUCTION

In this paper, we investigate the influence of paraboliclike approximations to the acoustic wave equations on the reflection of an impulsive, point-source generated, spherical acoustic wave at a plane interface between two different fluids. The direction of preference in the approximation is chosen normal to the interface. As such, it is representative for a seismiclike arrangement of sources and receivers rather than for wave propagation in an acoustic duct, where the direction of preference is customarily chosen parallel to the interfaces. Another difference is that the relevant acoustic wave guide problem is usually considered in the frequency domain, whereas our analysis is carried out in the time domain and focusses on transient phenomena.

As far as terminology is concerned, the pertaining approximations are denoted as "Taylor approximants," "Padé approximants," etc., partly depending on the kind of expansion of the wave operator involved. The work of Brezinski[1] reveals that Thiele (a Danish astronomer) was apparently the first to investigate approximations within the framework of constructing a general continued-fraction counterpart of the well-known (polynomial) Taylor expansion. For this reason, it would be appropriate to indicate the rational approximants as Thiele approximants. It is noted that the first-order Thiele and Taylor approximants necessarily coincide.

In the past, the first-order Thiele continued-fraction or standard parabolic approximation has been applied to various wave problems, amongst which are the propagation of waves in random media,[2,3] the downward continuation of acoustic waves in seismic prospecting,[4] and underwater acoustics.[5,6] In recent years, there is an increasing interest in the use of higher-order approximations (which include the Padé approximations). Thiele approximations have been either arrived at with the aid of a perturbation theory applied to the wave equation in a comoving frame of reference[7] or carried out on the wave function in the spectral domain.[8] They have been compared, in the spectral domain, with approximants of the vertical slowness obtained through least-squares fitting by Lee and Suh,[9] and through interpolation at a number of abcissa of the horizontal slowness by Halpern and Trefethen.[10]

The relation between the solutions of the exact (Helmholtz) and the first-order approximated (Schrödinger) equations for the propagation of sound in an acoustic wave guide has been analyzed, amongst others, by De Santo[11] and Collins.[12] Deviations, due to the approximation, in the phase and group velocities of normal modes in underwater acoustic ducts have been studied by McDaniel.[5] A comparison between the Green's functions of the scalar wave equation and its first- and second-order Thiele approximations in an unbounded domain has been carried out by De Hoop and De Hoop.[13] This paper also contains an extensive bibliography on the subject.

As the previous study[13] revealed that in an unbounded medium the Thiele approximation generates nonphysical,

[a)] Present address: Schlumberger Cambridge Research, High Cross, Madingley Road, Cambridge CB3 0EL, England.

[b)] Part of this work was done when the author was a Visiting Scientist with Schlumberger Cambridge Research, High Cross, Madingley Road, Cambridge CB3 0EL, England.

 0001-4966/93/010022-14$00.80

artificial "head waves," we presently extend the investigation to the higher-order approximation's capability to describe the real, physical head waves that occur in the wave reflection against the boundary with a medium with a higher wave speed. Upon evaluating the space-time Green's functions in the relevant two-media configuration it is found that, rather than generating the physical head wave, the Thiele approximation creates, in the reflection problem, additional artificial head-wavelike arrivals. Related approximations have been introduced by Richards and Frasier[14] and Shuey,[15] who combined it with a linearization of the reflection coefficients in the medium parameter contrasts across the interface.

The formalism for the first-order parabolic wave theory pertaining to media with interfaces across which the medium parameters jump by finite amounts has already been given by Corones[16] and McCoy *et al.*[17] Further, Hatton *et al.*[18] have analyzed the modification of Snell's law entailed by the first-order approximation for a two-media configuration (as represented by a transition zone).

Both the exact space-time solution to the problem and the solutions arising from the application of the first- and second-order Thiele approximations to the corresponding vertical slownesses are obtained with the aid of the modified Cagniard method.[13,19–22] For canonical problems of the type at hand, this method is still believed to be the most effective one as far as the accuracy of the space-time results and the computational effort involved are concerned. Due to its exact nature, the results also can serve as a check on the accuracy of purely numerical procedures by applying the latter to the configurations to which the modified Cagniard method applies. The method separates the total wave motion into a number of constituents each of which is of a particular nature. Also, it shows that the artifacts manifest themselves more clearly in the transient response than in its continuous-wave single-frequency counterpart. In addition, the analysis makes explicit in which regions of space and in which time interval the artifacts do occur and what their nature is.

I. THE TRANSFORM-DOMAIN WAVE MOTION

Consider linearized acoustic waves in an isotropic fluid occupying three-dimensional space $\mathscr{R}^3$. The point at which the wave motion is observed is specified by the coordinates $\{x_1,x_2,x_3\}$ with respect to a Cartesian reference frame with the origin $\mathscr{O}$ and three mutually perpendicular base vectors $\{\mathbf{i}_1,\mathbf{i}_2,\mathbf{i}_3\}$ each of unit length. In the indicated order, the base vectors form a right-handed system. In accordance with geophysical convention, x_3 (our direction of preference) is taken as the vertical, or depth, coordinate (which increases in the downward direction), leaving x_1,x_2 as the horizontal coordinates. The position vector will be denoted by $\mathbf{x}$. The time coordinate is denoted by t. Differentiation with respect to $x_{1,2,3}$ is denoted by $\partial_{1,2,3}$; ∂_t denotes differentiation with respect to t.

A. The basic acoustic equations

The acoustic wave motion is governed by the following system of first-order partial differential equations:

$$\partial_{1,2,3}p+\rho\,\partial_t v_{1,2,3}=f_{1,2,3}, \tag{1}$$

$$\kappa\,\partial_t p+\partial_1 v_1+\partial_2 v_2+\partial_3 v_3=q, \tag{2}$$

where p, the acoustic pressure, and $v_{1,2,3}$, the particle velocity, are the wave field quantities, ρ, the volume density of mass, and κ, the compressibility, are the acoustic fluid parameters, and q, the volume source density of injection rate (which models the action of a monopole transducer), and $f_{1,2,3}$, the volume source density of force (which models the action of a dipole transducer), are the source quantities.

Let the sources generating the wave field be switched on at the instant $t=0$, then causality implies that the wave-field quantities satisfy the initial conditions $p=0$ and $v_{1,2,3}=0$ for $t<0$ and all $\mathbf{x}$. In view of the time invariance of the medium, the causality of the wave motion can be taken into account by carrying out a one-sided Laplace transformation with respect to time, taking the time Laplace-transform parameter s, which is in general complex-valued, to be in the right half ($\mathrm{Re}\{s\}>0$) of the complex s plane and requiring that the transform-domain wave quantities are bounded functions of position in all space. To show the notation, we give the expression for the acoustic pressure

$$\hat{p}(\mathbf{x},s)=\int_{t=0}^{\infty}p(\mathbf{x},t)\exp(-st)dt. \tag{3}$$

Employing the translational invariance of the configuration in the horizontal directions, also a Fourier transformation is applied in the horizontal plane with real transform parameters $s\alpha_1$ and $s\alpha_2$. For the acoustic pressure, the relevant transformation is

$$\tilde{p}(i\alpha_{1,2},x_3,s)=\int_{x_{1,2}\in\mathscr{R}^2}\hat{p}(\mathbf{x},s)\times\exp[is(\alpha_1x_1+\alpha_2x_2)]dx_1\,dx_2. \tag{4}$$

The variables $i\alpha_{1,2}$ are the horizontal components of the slowness vector of the wave motion. The transformation inverse to Eq. (4) is given by

$$\hat{p}(\mathbf{x},s)=\left(\frac{s}{2\pi}\right)^2\int_{\alpha_{1,2}\in\mathscr{R}^2}\tilde{p}(i\alpha_{1,2},x_3,s)\times\exp[-is(\alpha_1x_1+\alpha_2x_2)]d\alpha_1\,d\alpha_2. \tag{5}$$

Under the Laplace transformation, assuming zero initial conditions, we have $\partial_t\to s$. The Fourier-domain counterpart of $\partial_{1,2}$ is given by $-is\alpha_{1,2}$. With these rules, the first-order acoustic wave equations (1) and (2) transform into

$$\partial_3\tilde{p}+s\rho\tilde{v}_3=\tilde{f}_3, \tag{6}$$

$$-is\alpha_{1,2}\tilde{p}+s\rho\tilde{v}_{1,2}=\tilde{f}_{1,2}, \tag{7}$$

$$s\kappa\tilde{p}-is(\alpha_1\tilde{v}_1+\alpha_2\tilde{v}_2)+\partial_3\tilde{v}_3=\tilde{q}. \tag{8}$$

B. The configuration

The configuration to be considered consists of two contiguous half-spaces, each filled with a homogeneous fluid. The interface between the half-spaces is located at a depth $x_3=h$. The half-space $x_3<h$ has the medium parameters ρ_1,κ_1; the half-space $x_3>h$ has the medium parameters ρ_2, κ_2. The source is a monopole point source at the origin; for this

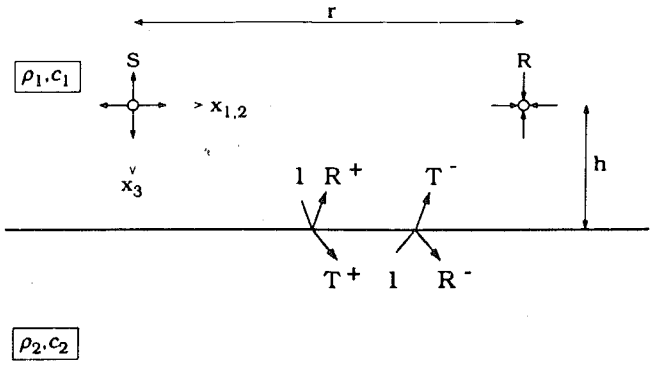

FIG. 1. The configuration of the reflection problem.

$$q = q^0(t)\delta(\mathbf{x}), \quad f_{1,2,3} = 0, \tag{9}$$

in which $q^0(t)$ is the source signature and $\delta(\mathbf{x})$ is the three-dimensional Dirac distribution operative at $\mathbf{x} = \mathbf{0}$. Accordingly,

$$\tilde{q} = \hat{q}^0(s)\delta(x_3), \quad \tilde{f}_{1,2,3} = 0. \tag{10}$$

The receiver that detects the pressure is located at a depth $x_3 < h$ (see Fig. 1; $R^{\pm}$ denote the reflection coefficients and $T^{\pm}$ denote the transmission coefficients). Across the interface separating the half-spaces, $\tilde{p}$ and $\tilde{v}_3$ are to be continuous.

C. The transform-domain incident field

From Eqs. (6)–(8) and (10), the transform-domain incident pressure field in the half-space $x_3 < h$ is found as

$$\tilde{p}_i = (2Y_1)^{-1}\hat{q}^0(s)\exp(-s\gamma_1|x_3|), \tag{11}$$

where

$$\gamma_1 = (c_1^{-2} + \alpha_1^2 + \alpha_2^2)^{1/2} \tag{12}$$

is the vertical slowness and

$$Y_1 = \gamma_1/\rho_1 \tag{13}$$

is the vertical acoustic wave admittance. The Green's function associated with the incident pressure is then given by

$$\tilde{G}_i = (2s^2Y_1)^{-1}\exp(-s\gamma_1|x_3|), \quad -\infty < x_3 < h. \tag{14}$$

Note that this function has been chosen to contain a factor s^{-2} that compensates the factor s^2 in the inverse Fourier transformation Eq. (5).

D. The transform-domain reflected field

The transform-domain reflected pressure field in the half-space $x_3 < h$ takes the form

$$\tilde{p}_r = (2Y_1)^{-1}\hat{q}^0(s)R\exp[-s\gamma_1(2h - x_3)], \tag{15}$$

where

$$R = R^+ = -(Y_2 - Y_1)/(Y_2 + Y_1) \tag{16}$$

is the reflection coefficient with

$$Y_2 = \gamma_2/\rho_2 \tag{17}$$

and

$$\gamma_2 = (c_2^{-2} + \alpha_1^2 + \alpha_2^2)^{1/2}. \tag{18}$$

The Green's function associated with the reflected pressure is then given by

$$\tilde{G}_r = (2s^2Y_1)^{-1}R\exp[-s\gamma_1(2h - x_3)], \quad -\infty < x_3 < h. \tag{19}$$

The two space-time Green's functions G_i and G_r will next be analyzed in detail, both exactly and in their first- and second-order Thiele (parabolic) approximations.

E. The general Green's tensor

The general acoustic Green's tensor associated with a vertically inhomogeneous configuration consists of the acoustic pressure and the vertical particle velocity due to both a point source of volume injection (monopole source) and a vertical point force (vertical dipole source). It contains four elements each of which can be expressed in terms of $\tilde{G}_i$ and $\tilde{G}_r$. We write the transform-domain Green's tensor as

$$\tilde{\mathbf{G}} = \begin{pmatrix} \tilde{G}^{pf} & \tilde{G}^{pq} \\ \tilde{G}^{vf} & \tilde{G}^{vq} \end{pmatrix}, \tag{20}$$

where the first superscript refers to the type of observed quantity $(\tilde{p},\tilde{v}_3)$ and the second superscript refers to the type of source $(\tilde{f}_3,\tilde{q})$. From Eqs. (6)–(8), it is found that, upon separating into incident and reflected wave field contributions,

$$\tilde{\mathbf{G}} = \tilde{\mathbf{G}}_i + \tilde{\mathbf{G}}_r, \quad -\infty < x_3 < h, \tag{21}$$

with

$$\tilde{\mathbf{G}}_i = \mathscr{D}_i\tilde{G}_i + \begin{pmatrix} 0 & 0 \\ \rho_1^{-1}s^{-3}\delta(x_3) & 0 \end{pmatrix}, \quad \tilde{\mathbf{G}}_r = \mathscr{D}_r\tilde{G}_r, \tag{22}$$

in which $\mathscr{D}_i$ and $\mathscr{D}_r$ are the operators

$$\mathscr{D}_i = \begin{pmatrix} -\rho_1^{-1}s^{-1}\partial_3 & 1 \\ (\rho_1^{-1}s^{-1}\partial_3)^2 & -\rho_1^{-1}s^{-1}\partial_3 \end{pmatrix}, \quad \mathscr{D}_r = \begin{pmatrix} \rho_1^{-1}s^{-1}\partial_3 & 1 \\ (\rho_1^{-1}s^{-1}\partial_3)^2 & \rho_1^{-1}s^{-1}\partial_3 \end{pmatrix}. \tag{23}$$

II. THE GREEN'S FUNCTIONS IN THE TIME-LAPLACE DOMAIN

The first step toward the construction of the solution in the space-time domain with the aid of the modified Cagniard method consists of carrying out the inverse transformation Eq. (5). In this integral the variables of integration $\{\alpha_1,\alpha_2\}$ with $\{\alpha_1 \in \mathscr{R}, \alpha_2 \in \mathscr{R}\}$ are transformed into $\{p,q\}$ with $\{p \in \mathscr{I}, q \in \mathscr{R}\}$ (here $\mathscr{R}$ denotes the real axis and $\mathscr{I}$ denotes the imaginary axis) through (De Hoop[19])

$$\alpha_1 = -ip\cos(\phi) - q\sin(\phi), \quad \alpha_2 = -ip\sin(\phi) + q\cos(\phi), \tag{24}$$

where $\{r,\phi\}$ is related to $\{x_1,x_2\}$ by

$$x_1 = r\cos(\phi), \quad x_2 = r\sin(\phi), \tag{25}$$

with $0 \leqslant r < \infty$, $0 \leqslant \phi < 2\pi$. With this

$$\alpha_1 x_1 + \alpha_2 x_2 = pr, \tag{26}$$

$$\alpha_1^2 + \alpha_2^2 = q^2 - p^2. \tag{27}$$

Next, while q is kept real, the resulting integrand is continued analytically into the complex p plane. Subsequently, the integration is carried out along the modified Cagniard path that follows from a continuous deformation of the imaginary p axis and changes the exponential function in the integrand into $\exp(-s\tau)$, where τ is the real and positive travel time parameter along the path. Introducing in the integral with respect to p, τ as the variable of integration and interchanging the integrations with respect to τ and q, we end up with a Laplace integral with respect to time, the integrand of which is the desired time-domain result. Lerch's theorem (Widder[23]) ensures that this procedure is unique. Experience with some exact solutions (see, for example, De Hoop and Van der Hijden[24]) shows that the nature and the location of the singularities in the complex p plane are indicative for the presence of certain constituents in the wave motion. So, open modified Cagniard paths extending to infinity correspond to body waves, looplike paths around branch cuts associated with square-root expressions for the vertical slownesses and wave admittances correspond to head waves, while poles correspond to surface waves. Further, in the exact solution no singularities in space show up in the wave motion, except at the source point. Now, in the parabolic approximations the branch points (and the associated branch cuts) will be shown to disappear, while extra poles show up. This raises the question, how far the contributions from the poles take over, in the parabolic approximations, the phenomenon of the occurrence of head waves in the exact wave motion. In addition, the second-, as well as all even higher-order approximations lead to divergent integrals (and corresponding singularities in the integrand at infinity in the complex p plane), that somehow must be interpreted and that will be shown to lead to nonphysical singular points outside the sources as artifacts in space. In those regions of space where such drastic artifacts show up, the parabolic approximations are clearly outside their region of applicability. The associated phenomena occur at relatively large source–receiver horizontal offsets, which may arise in a surface seismic exploration setting. Further, it will be shown that the approximative nature of the parabolic approximations is more manifest in the transient signal than in its single-frequency continuous-wave counterpart. For this reason, the emphasis in our analysis is on the time-domain results.

Since through the parabolic approximations the nature of the singularities in the complex p plane has been changed (single branch points are replaced by several poles), and, further, the asymptotic behavior as $|p|\to\infty$ is modified, the resulting wave motion is, apart from being approximative in some sense, also expected to be provided with artifacts that are totally unrelated to the exact physical wave motion.

Application of the inverse Fourier transformation Eq. (5) to Eqs. (14) and (19) yields

$$\hat{G}_i(x_{1,2},x_3,s)=\rho_1(4\pi^2)^{-1}\int_{\alpha_{1,2}\in\mathscr{R}^2}(2\gamma_1)^{-1}\times\exp[-is(\alpha_1x_1+\alpha_2x_2)]\times\exp(-s\gamma_1|x_3|)\,d\alpha_1\,d\alpha_2, \tag{28}$$

$$\hat{G}_r(x_{1,2},x_3,s)=\rho_1(4\pi^2)^{-1}\int_{\alpha_{1,2}\in\mathscr{R}^2}(2\gamma_1)^{-1}R\times\exp[-is(\alpha_1x_1+\alpha_2x_2)]\times\exp[-s\gamma_1(2h-x_3)]\,d\alpha_1\,d\alpha_2. \tag{29}$$

To construct the time-domain equivalents of $\hat{G}_i$ and $\hat{G}_r$, and hence of $\hat{\mathbf{G}}_i$ and $\hat{\mathbf{G}}_r$, the modified Cagniard method is applied.

After transforming the variables according to Eq. (24), we obtain for the incident and reflected field Green's functions the expressions

$$\hat{G}_i=\frac{1}{4\pi^2i}\int_{q=-\infty}^{\infty}dq\int_{p=-i\infty}^{i\infty}\mathscr{F}_i(p,q)\times\exp[-s(pr+\gamma_1|x_3|)]dp,$$
$$\hat{G}_r=\frac{1}{4\pi^2i}\int_{q=-\infty}^{\infty}dq\int_{p=-i\infty}^{i\infty}\mathscr{F}_r(p,q)\times\exp\{-s[pr+\gamma_1(2h-x_3)]\}dp, \tag{30}$$

in which

$$\mathscr{F}_i(p,q)=\frac{\rho_1}{2\gamma_1(p,q)},\quad \mathscr{F}_r(p,q)=\mathscr{F}_i(p,q)R. \tag{31}$$

Further details of the method are given in Appendices A and B.

III. THE EXACT GREEN'S FUNCTIONS IN THE TIME DOMAIN

In this section we present the exact Green's functions in the space-time domain.

A. The incident field Green's function

The exact Green's function for the incident wave has been determined in De Hoop and De Hoop[13] and is given by

$$G_i=\frac{\rho_1}{4\pi R}H\left(t-\frac{R}{c_1}\right), \tag{32}$$

where $R=(x_1^2+x_2^2+x_3^2)^{1/2}$ is the distance from the source to the receiver.

B. The reflected field Green's function

For the exact reflected field the modified Cagniard path follows from Eq. (A1) with $\gamma=\gamma_1$ and $H=2h-x_3$. We will consider the case $c_1<c_2$; then, head waves occur in addition to the body waves. The body-wave part of contour in the first quadrant is given by (see also De Hoop and Van der Hijden[24])

$$p^{\mathrm{BW}}=(1/R^2)\{r\tau+iH[\tau^2-T_{\mathrm{BW}}^2(q)]^{1/2}\}$$

when

$$T_{\mathrm{BW}}(q)<\tau<\infty, \tag{33}$$

while the head-wave part of the contour (loop around the branch cut) is given by

$$p^{\mathrm{HW}}=(1/R^2)\{r\tau-H[T_{\mathrm{BW}}^2(q)-\tau^2]^{1/2}\}$$

when

$$T_{\mathrm{HW}}(q) < \tau < T_{\mathrm{BW}}(q), \tag{34}$$

where

$$T_{\mathrm{BW}}(q) = R(c_1^{-2} + q^2)^{1/2}, \tag{35}$$

$$T_{\mathrm{HW}}(q) = r(c_2^{-2} + q^2)^{1/2} + H(c_1^{-2} - c_2^{-2})^{1/2}, \tag{36}$$

in which

$$R = (r^2 + H^2)^{1/2} \tag{37}$$

is now the distance from the image of the source in the reflecting interface to the receiver. The inverse relationships of Eqs. (35) and (36) follow as

$$Q_{\mathrm{BW}}(\tau) = (1/R)(\tau^2 - R^2/c_1^2)^{1/2}, \tag{38}$$

$$Q_{\mathrm{HW}}(\tau) = \left[\left(\frac{\tau - H(c_1^{-2} - c_2^{-2})^{1/2}}{r}\right)^2 - \frac{1}{c_2^2}\right]^{1/2}. \tag{39}$$

It is observed that $Q_{\mathrm{BW}}(\tau) \leqslant Q_{\mathrm{HW}}(\tau)$ when $\tau \in [T_{\mathrm{BW}}(0), T]$, with

$$T = (R^2/H)(c_1^{-2} - c_2^{-2})^{1/2}. \tag{40}$$

Notice that the situation $T_{\mathrm{BW}}(0) < T$ only occurs outside the cone $r/H > [(c_2/c_1)^2 - 1]^{-1/2}$ where the head wave exists. The one-dimensional Jacobians corresponding to Eqs. (33)–(34) follow as

$$\frac{\partial p^{\mathrm{BW}}}{\partial \tau} = i[\tau^2 - T_{\mathrm{BW}}^2(q)]^{-1/2}\gamma_1(p^{\mathrm{BW}}, q), \tag{41}$$

$$\frac{\partial p^{\mathrm{HW}}}{\partial \tau} = [T_{\mathrm{BW}}^2(q) - \tau^2]^{-1/2}\gamma_1(p^{\mathrm{HW}}, q), \tag{42}$$

in which

$$\gamma_1(p^{\mathrm{BW}}, q) = (1/R^2)\{H\tau - ir[\tau^2 - T_{\mathrm{BW}}^2(q)]^{1/2}\}, \tag{43}$$

when $T_{\mathrm{BW}}(q) < \tau < \infty$, and

$$\gamma_1(p^{\mathrm{HW}}, q) = (1/R^2)\{H\tau + r[T_{\mathrm{BW}}^2(q) - \tau^2]^{1/2}\}, \tag{44}$$

when $T_{\mathrm{HW}}(q) < \tau < T_{\mathrm{BW}}(q)$. It is noted that

$$\tau^2 - T_{\mathrm{BW}}^2(q) = R^2[Q_{\mathrm{BW}}^2(\tau) - q^2]. \tag{45}$$

Following the analysis of Appendix A, the exact reflected field Green's function is found to be

$$\begin{aligned} G_r = {} & \left\{\pi^{-2}\rho_1 \int_{q=0}^{Q_{\mathrm{HW}}(t)} \mathrm{Im}\left[\left(\frac{R}{2\gamma_1}\right)\left(\frac{\partial p}{\partial t}\right)\right]_{p^{\mathrm{HW}}} dq\right\}\chi_{[T_{\mathrm{HW}}(0), T_{\mathrm{BW}}(0)]}(t) \\ & + \left\{\pi^{-2}\rho_1 \int_{q=Q_{\mathrm{BW}}(t)}^{Q_{\mathrm{HW}}(t)} \mathrm{Im}\left[\left(\frac{R}{2\gamma_1}\right)\left(\frac{\partial p}{\partial t}\right)\right]_{p^{\mathrm{HW}}} dq + \pi^{-2}\rho_1 \int_{q=0}^{Q_{\mathrm{BW}}(t)} \mathrm{Im}\left[\left(\frac{R}{2\gamma_1}\right)\left(\frac{\partial p}{\partial t}\right)\right]_{p^{\mathrm{BW}}} dq\right\}\chi_{[T_{\mathrm{BW}}(0), T]}(t) \\ & + \left\{\pi^{-2}\rho_1 \int_{q=0}^{Q_{\mathrm{BW}}(t)} \mathrm{Im}\left[\left(\frac{R}{2\gamma_1}\right)\left(\frac{\partial p}{\partial t}\right)\right]_{p^{\mathrm{BW}}} dq\right\}H(t - T), \end{aligned} \tag{46}$$

in which χ denotes the characteristic function. The integrals are evaluated numerically. In Figs. 2 and 3, a near horizontal offset (precritical angle of incidence) and a far horizontal offset (postcritical angle of incidence) trace, corresponding to the exact Green's function, are shown ($h = 500$ m; $r = 500$ m, corresponding to an angle of incidence of about 26°, and $r = 1750$ m, corresponding to an angle of incidence of about 60°, respectively).

IV. THE RATIONAL PARABOLIC APPROXIMATIONS FOR THE SLOWNESS AND THE REFLECTION COEFFICIENT

In this section we give, as a preliminary to the first- and second-order rational parabolic approximations to the wave

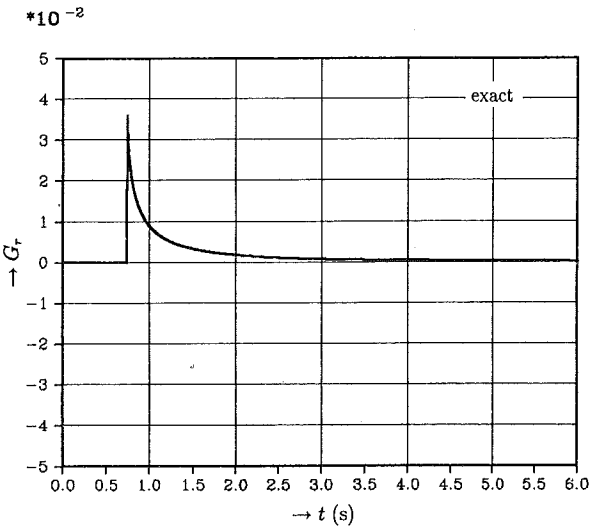

FIG. 2. The exact reflected-wave Green's function when $r = 500$ m and $h = 500$ m. The medium parameters are $\rho_1 = \rho_2 = 1000$ kg/m^3, $c_1 = 1500$ m/s, and $c_2 = 2828$ m/s.

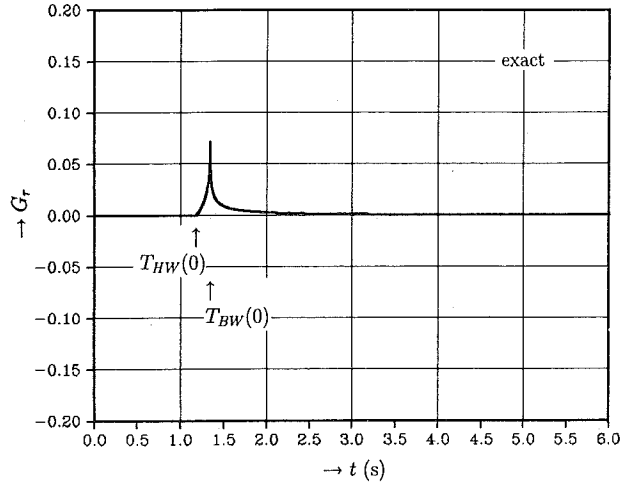

FIG. 3. The exact reflected-wave Green's function when $r = 1750$ m and $h = 500$ m. The medium parameters are $\rho_1 = \rho_2 = 1000$ kg/m^3, $c_1 = 1500$ m/s, and $c_2 = 2828$ m/s.

motion, the relevant approximations to the vertical slownesses, the vertical wave admittances, and the reflection coefficient. The first- and second-order approximations are denoted by the superscripts I and II, respectively. At this point it is noted that, as has been shown in a previous paper,[13] all higher-order approximations lead to a succession of terms in γ_m, $m = 1,2$, each of which has the shape of either a first- or a second-order approximation.

A. The first-order approximation

In the first-order approximation,[4] we have

$$\gamma_m^{\mathrm{I}} = c_m^{-1} + (c_m/2)(q^2 - p^2),$$
$$Y_m^{\mathrm{I}} = \gamma_m^{\mathrm{I}}/\rho_m = (\rho_m c_m)^{-1}[1 + (c_m^2/2)(q^2 - p^2)], \quad \text{for } m = 1,2. \tag{47}$$

Due to the occurrence of the factor $1/2\gamma_1^{\mathrm{I}}$ in both $\tilde{G}_i^{\mathrm{I}}$ and $\tilde{G}_r^{\mathrm{I}}$, these functions contain a simple pole at

$$p_0^{\mathrm{I}}(q) = [q^2 + 2/c_1^2]^{1/2}. \tag{48}$$

With Eq. (47), the expression for the reflection coefficient becomes

$$R^{\mathrm{I}} = -\frac{(\rho_2 c_2)^{-1} - (\rho_1 c_1)^{-1} + (1/2)[(c_2/\rho_2) - (c_1/\rho_1)](q^2 - p^2)}{(\rho_2 c_2)^{-1} + (\rho_1 c_1)^{-1} + (1/2)[(c_2/\rho_2) + (c_1/\rho_1)](q^2 - p^2)}. \tag{49}$$

This contains simple poles at the simple zeros of its denominator. In the right half of the complex p plane, these are given by

$$p_R^{\mathrm{I}}(q) = (q^2 + 2/\langle c\rangle_{\mathrm{I}}^2)^{1/2}, \tag{50}$$

in which

$$\langle c\rangle_{\mathrm{I}}^{-2} = \frac{1}{c_1^2}\left(\frac{1 + (\rho_1 c_1/\rho_2 c_2)}{1 + (\rho_1 c_2/\rho_2 c_1)}\right). \tag{51}$$

The following situations occur:

$$c_1/c_2 < 1 \quad \text{then} \quad \langle c\rangle_{\mathrm{I}}^{-2} < c_1^{-2}, \tag{52}$$
$$c_1/c_2 = 1 \quad \text{then} \quad \langle c\rangle_{\mathrm{I}}^{-2} = c_1^{-2}, \tag{53}$$
$$c_1/c_2 > 1 \quad \text{then} \quad \langle c\rangle_{\mathrm{I}}^{-2} > c_1^{-2}. \tag{54}$$

In the case $c_1 = c_2$, the pole actually vanishes and the reflection coefficient reduces to the exact expression $R^{\mathrm{I}} = -(\rho_2^{-1} - \rho_1^{-1})/(\rho_1^{-1} + \rho_2^{-1})$. (When, in addition, $\rho_1 = \rho_2$, the reflection coefficient vanishes.) Note that in the first-order approximation no branch points occur.

B. The second-order approximation

In the second-order approximation,[8] we have

$$\gamma_m^{\mathrm{II}} = \frac{3}{c_m}\left(\frac{4/3c_m^2 + (q^2 - p^2)}{4/c_m^2 + (q^2 - p^2)}\right),$$
$$Y_m^{\mathrm{II}} = \gamma_m^{\mathrm{II}}/\rho_m = 3(\rho_m c_m)^{-1}\left(\frac{4/3c_m^2 + (q^2 - p^2)}{4/c_m^2 + (q^2 - p^2)}\right), \quad \text{for } m = 1,2. \tag{55}$$

Due to the occurrence of the factor $1/2\gamma_1^{\mathrm{II}}$ in both $\tilde{G}_i^{\mathrm{II}}$ and $\tilde{G}_r^{\mathrm{II}}$, these functions contain, in the right half of the complex p plane, a simple pole at

$$p_0^{\mathrm{II}}(q) = (q^2 + 4/3c_1^2)^{1/2}. \tag{56}$$

The expression for the reflection coefficient now becomes

$$R^{\mathrm{II}} = -E^-/E^+, \tag{57}$$

where

$$E^{\pm} = (\rho_2 c_2)^{-1}[4/3c_2^2 + (q^2 - p^2)][4/c_1^2 + (q^2 - p^2)] \pm (\rho_1 c_1)^{-1}[4/3c_1^2 + (q^2 - p^2)] \times [4/c_2^2 + (q^2 - p^2)]. \tag{58}$$

This contains simple poles at the zeros of its denominator. In the right half of the complex p plane, these are given by

$$p_{R,1,2}^{\mathrm{II}}(q) = (q^2 + 4/3\langle c\rangle_{\mathrm{II};1,2}^2)^{1/2}, \tag{59}$$

in which

$$\langle c\rangle_{\mathrm{II};1}^{-2} = c_1^{-2}[Q - (Q^2 - P)^{1/2}], \tag{60}$$
$$\langle c\rangle_{\mathrm{II};2}^{-2} = c_1^{-2}[Q + (Q^2 - P)^{1/2}], \tag{61}$$

where

$$P = 3(c_1/c_2)^2 \tag{62}$$

and

$$Q = \frac{1}{2}\left(\frac{1 + 3(\rho_1 c_1/\rho_2 c_2) + (c_1/c_2)^2[3 + (\rho_1 c_1/\rho_2 c_2)]}{1 + (\rho_1 c_1/\rho_2 c_2)}\right). \tag{63}$$

Notice that $Q^2 > P$, since the volume densities of mass and the wave speeds are real and positive. The following situations occur:

$$c_1/c_2 < 1 \quad \text{then} \quad \langle c\rangle_{\mathrm{II};1}^{-2} < c_1^{-2} \quad \text{and} \quad c_1^{-2} < \langle c\rangle_{\mathrm{II};2}^{-2} < 3c_1^{-2}, \tag{64}$$
$$c_1/c_2 = 1 \quad \text{then} \quad \langle c\rangle_{\mathrm{II};1}^{-2} = c_1^{-2} \quad \text{and} \quad \langle c\rangle_{\mathrm{II};2}^{-2} = 3c_1^{-2}, \tag{65}$$
$$c_1/c_2 > 1 \quad \text{then} \quad c_1^{-2} < \langle c\rangle_{\mathrm{II};1}^{-2} < 3c_1^{-2} \quad \text{and} \quad 3c_1^{-2} < \langle c\rangle_{\mathrm{II};2}^{-2}. \tag{66}$$

In the case $c_1 = c_2$, the poles actually vanish and the reflec-

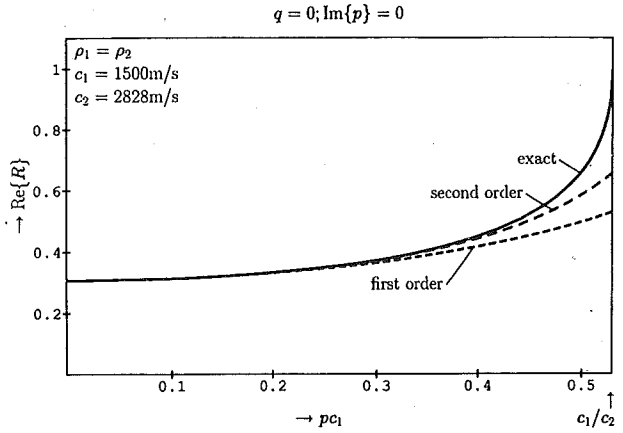

FIG. 4. The real parts of the exact and first- and second-order approximated reflection coefficients on the real p axis up to the critical angle of incidence; $q = 0$. The medium parameters are $\rho_1 = \rho_2 = 1000\,\mathrm{kg/m^3}$, $c_1 = 1500\,\mathrm{m/s}$, and $c_2 = 2828\,\mathrm{m/s}$.

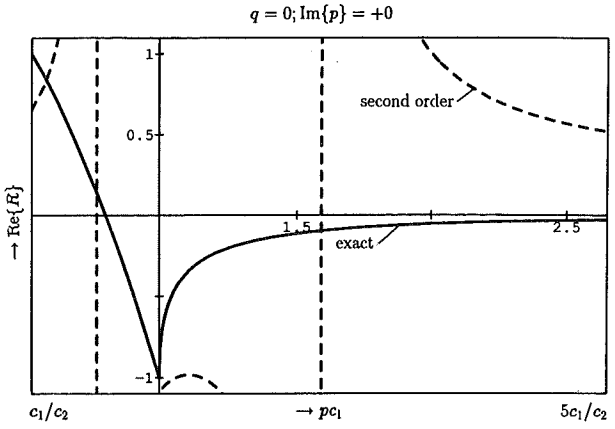

FIG. 6. The real parts of the exact and second-order approximated reflection coefficients on the real p axis from the critical angle of incidence onward; $q = 0$. The medium parameters are $\rho_1 = \rho_2 = 1000\ \mathrm{kg/m^3}$, $c_1 = 1500\,\mathrm{m/s}$, and $c_2 = 2828\,\mathrm{m/s}$.

tion coefficient reduces to the exact expression $R^{\mathrm{II}} = -(\rho_2^{-1} - \rho_1^{-1})/(\rho_1^{-1} + \rho_2^{-1})$. (When, in addition, $\rho_1 = \rho_2$, the reflection coefficient vanishes.) Note that in this approximation no branch points occur. In Figs. 3–7, the exact and approximate reflection coefficients are shown for different ranges of the horizontal slowness.

V. THE CAGNIARD PATH CONTRIBUTIONS TO THE APPROXIMATED GREEN'S FUNCTIONS

In this section, we determine the Cagniard path contributions to the approximated Green's functions.

A. The first-order approximation

For the first-order approximation, γ_1 in Eq. (A1) is replaced by γ_1^{I} according to Eq. (47). Solving for p from the resulting equation, it is found that the modified Cagniard path consists of $p = p^{\mathrm{I}}(\tau,q)$ in the first quadrant of the complex p plane, together with its complex conjugate $p = p^{\mathrm{I}*}(\tau,q)$ in the fourth quadrant of the complex p plane, where

$$p^{\mathrm{I}} = (r/c_1 H) + i(2/c_1 H)^{1/2}[\tau - T^{\mathrm{I}}(q)]^{1/2} \quad \text{for } T^{\mathrm{I}}(q) \leqslant \tau < \infty, \tag{67}$$

in which

$$T^{\mathrm{I}}(q) = T^{\mathrm{I}}(0) + (c_1 H/2)q^2, \tag{68}$$

with

$$T^{\mathrm{I}}(0) = (H/c_1)(1 + r^2/2H^2). \tag{69}$$

Equation (67) represents a straight line parallel to the imaginary p axis that intersects the real p axis at $p = r/c_1 H$. Along this path, τ strictly increases when going from the point of intersection with the real p axis to infinity. Then, the

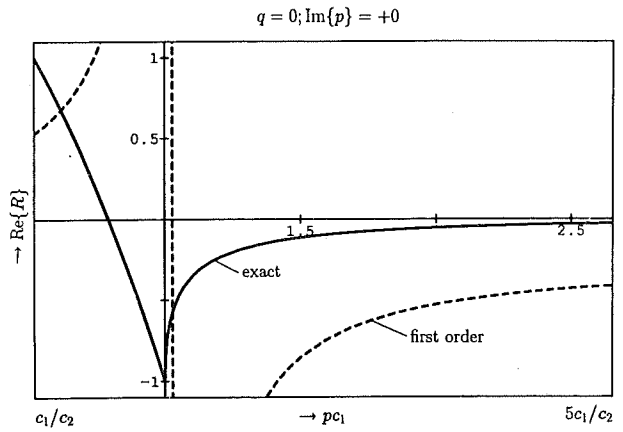

FIG. 5. The real parts of the exact and first-order approximated reflection coefficients on the real p axis from the critical angle of incidence onward; $q = 0$. The medium parameters are $\rho_1 = \rho_2 = 1000\,\mathrm{kg/m^3}$, $c_1 = 1500\,\mathrm{m/s}$, and $c_2 = 2828\,\mathrm{m/s}$.

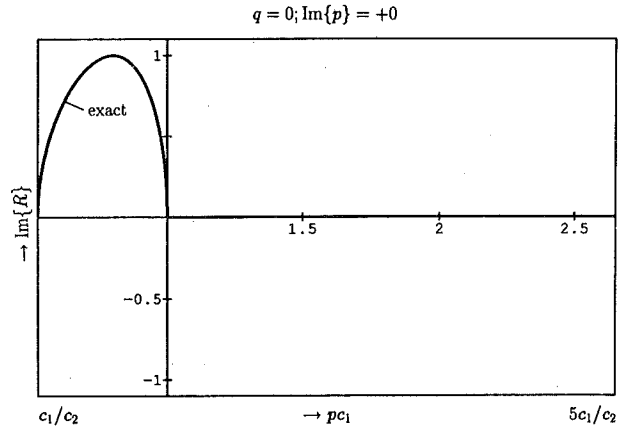

FIG. 7. The imaginary parts of the exact and first- and second-order approximated reflection coefficients on the real p axis from the critical angle of incidence onward; $q = 0$. The medium parameters are $\rho_1 = \rho_2 = 1000\ \mathrm{kg/m^3}$, $c_1 = 1500\,\mathrm{m/s}$, and $c_2 = 2828\,\mathrm{m/s}$.

integral along the imaginary p axis is equal to the integral along the modified Cagniard path, apart from possible pole contributions which will be discussed in the next section. In the resulting integral, τ is introduced as the variable of integration. The corresponding one-dimensional Jacobian follows from Eq. (67) as

$$\frac{\partial p^{\mathrm{I}}}{\partial \tau} = i(2c_1 H)^{-1/2}[\tau - T^{\mathrm{I}}(q)]^{-1/2}. \tag{70}$$

Proceeding as outlined in Appendix A, we obtain for the Cagniard path contribution $G^{\mathrm{I}}_{i,r;C}$ to the first-order approximated Green's functions the expression

$$G^{\mathrm{I}}_{i,r;C} = \left\{\pi^{-2}\int_{q=0}^{Q^{\mathrm{I}}(t)} \mathrm{Im}\left[\mathscr{F}^{\mathrm{I}}_{i,r}(p^{\mathrm{I}}(t,q),q)\left(\frac{\partial p^{\mathrm{I}}}{\partial t}\right)\right] dq\right\} \times H[t - T^{\mathrm{I}}(0)], \tag{71}$$

in which $q = Q^{\mathrm{I}}(\tau)$ is the (unique) inverse of $\tau = T^{\mathrm{I}}(q)$ and is given by

$$Q^{\mathrm{I}}(\tau) = (2/c_1 H)^{1/2}[\tau - T^{\mathrm{I}}(0)]^{1/2}, \tag{72}$$

where $H = |x_3|$ for the incident wave and $H = 2h - x_3$ for the reflected wave. From Eq. (71), it is evident that $T^{\mathrm{I}}(0)$ as given by Eq. (69) is the arrival time of the wave. Through the substitution given in Eq. (A5) with $Q_1 = Q^{\mathrm{I}}$ and $Q_2 = 0$, the integral in Eq. (71) can be evaluated in closed form for the incident wave (for the scalar wave problem in an unbounded homogeneous medium, see De Hoop and De Hoop[13]) and numerically for the reflected wave.

B. The second-order approximation

For the second-order approximation, γ_1 in Eq. (A1) is replaced by γ_1^{II} according to Eq. (55), which is rewritten as

$$\gamma_1^{\mathrm{II}} = \frac{3}{c_1}\left(1 - \frac{A^2}{B^2(q) - p^2}\right), \tag{73}$$

with

$$A^2 = 8/3c_1^2, \quad B^2(q) = q^2 + 4/c_1^2. \tag{74}$$

Before proceeding as in Appendix A, it is observed, however, that upon replacing γ_1 in any element of the Green's tensor by γ_1^{II}, the inversion integral Eq. (30) becomes divergent since $\gamma_1^{\mathrm{II}} \to 3/c_1$ as $\alpha_1^2 + \alpha_2^2 \to \infty$, and a physically meaningful interpretation of the integral must be found. The asymptotic structure of the integrands in Eqs. (28) and (29) as $\alpha_1^2 + \alpha_2^2 \to \infty$ leads to the conjecture that the divergent integral contains a contribution that could be interpreted as a Dirac delta distribution operative at the vertical line $\{x_1 = 0, x_2 = 0\}$. In view of this and of the contour deformation to follow, it is assumed that an interpretation in the sense of a Cauchy principal value around infinity will lead to an acceptable result. Adopting this interpretation, the integrals on the right-hand sides of Eqs. (28) and (29) are replaced by the limit of the integrals over the rectangle $\{\alpha_1 \in \mathscr{R}, \alpha_2 \in \mathscr{R}; -\Delta_{\alpha_1} < \alpha_1 < \Delta_{\alpha_1}, -\Delta_{\alpha_2} < \alpha_2 < \Delta_{\alpha_2}\}$ with $\Delta_{\alpha_1} \to \infty$ and $\Delta_{\alpha_2} \to \infty$. In accordance with this, the inversion integral is, after the change of variables Eq. (24), interpreted as a limiting integral over the rectangle $\{q \in \mathscr{R}; -\Delta < q < \Delta\}$ and $\{p \in \mathscr{I}; -i\Delta < p < i\Delta\}$ with $\Delta \to \infty$.

The contour deformation leading from the integration along the imaginary p axis to the one along the modified Cagniard path is next analyzed. The latter path is the non-real-axis part of the solution to the cubic equation resulting from Eqs. (A1) and (73) along which τ strictly increases. This part consists of $p = p^{\mathrm{II}}(\tau,q)$ in the first quadrant of the complex p plane, together with its complex conjugate $p = p^{\mathrm{II}*}(\tau,q)$ in the fourth quadrant of the complex p plane. Its explicit form is obtained from Cardano's formula for the solution of the algebraic cubic equation; the relevant expression is given in a previous paper.[13] Here, we need some properties of the modified Cagniard path $\{p = p^{\mathrm{II}}(\tau,q) \cup p = p^{\mathrm{II}*}(\tau,q)\}$. It follows that $p = p^{\mathrm{II}}(\tau,q)$ and $p = p^{\mathrm{II}*}(\tau,q)$ are finite arcs that leave the real p axis at $p_1^{\mathrm{II}}(q)$, at which point the value of τ is denoted by $T_1^{\mathrm{II}}(q)$, and return to the real p axis again at $p_2^{\mathrm{II}}(q)$, at which point the value of τ is denoted by $T_2^{\mathrm{II}}(q)$. Inspection of the behavior of τ as a function of p along the real p-axis reveals that $p_1^{\mathrm{II}}(q) < B(q)$ and $p_2^{\mathrm{II}}(q) > B(q)$. Note that the points $p_{1,2}^{\mathrm{II}}(q)$ must be double roots of the relevant path equation. Thus, using the theory of resultants[25] to obtain the condition for the existence of a common root of the path equation following from Eq. (A1) and the equation $\partial\tau/\partial p = 0$, it is found that

$$\left(\frac{4}{3}B^2(q) + \frac{3\xi A^2}{2(T^{\mathrm{II}}(q) - \xi)}\right)^2 - 4\left(\frac{B^4(q)r}{6(T^{\mathrm{II}}(q) - \xi)} + \frac{B^2(q)(T^{\mathrm{II}}(q) - \xi)}{2r} + \frac{\xi A^2}{2r}\right) \times \left(\frac{T^{\mathrm{II}}(q) - \xi}{6r} + \frac{B^2(q)r}{2(T^{\mathrm{II}}(q) - \xi)}\right) = 0, \tag{75}$$

where $\xi = 3H/c_1$. This equation is quartic in $T^{\mathrm{II}}(q)$.

Now, in view of Cauchy's theorem, the integral along the imaginary p axis is equal to the sum of the integrals along the semi-circle $\mathscr{C}_\Delta^+ = \{p \in \mathscr{C}; |p| = \Delta, \mathrm{Re}(p) > 0\}$ and the modified Cagniard path. (The pole contributions are discussed in the next section.) On $\mathscr{C}_\Delta^+$ the integrand is asymptotically equal to $\tilde{G}^{\mathrm{II}}_{i,r;\infty} = (1/s^2)\mathscr{F}_{i,r;\infty} \times \exp[-s(pr - 3H/c_1)]$ in which $\mathscr{F}_{i,r;\infty}$ is the finite limit $\mathscr{F}_{i,r;\infty} = \lim_{p\to\infty} \mathscr{F}^{\mathrm{II}}_{i,r}(p,q)$. Using the asymptotic integrand $\tilde{G}^{\mathrm{II}}_{i,r;\infty}$, and carrying out the transformation inverse to Eq. (24), it follows that the contribution of $\mathscr{C}_\Delta^+$ results in

$$\lim_{\Delta_{\alpha_1}\to\infty, \Delta_{\alpha_2}\to\infty}\left(\frac{s}{2\pi}\right)^2 \int_{\alpha_1 = -\Delta_{\alpha_1}}^{\Delta_{\alpha_1}} d\alpha_1 \times \int_{\alpha_2 = -\Delta_{\alpha_2}}^{\Delta_{\alpha_2}} \exp[-is(\alpha_1 x_1 + \alpha_2 x_2)] \times \left(\frac{1}{s^2}\right)\mathscr{F}_{i,r;\infty} \exp\left(\frac{-3sH}{c_1}\right) d\alpha_2 = (1/s^2)\mathscr{F}_{i,r;\infty} \exp(-3sH/c_1)\delta(x_1,x_2). \tag{76}$$

Proceeding further as outlined in Appendix A, the contour contribution $G^{\mathrm{II}}_{i,r;C}$ to the approximated Green's functions is obtained as

$$G^{\mathrm{II}}_{i,r;C} = \mathscr{F}_{i,r;\infty}\left(t-\frac{3H}{c_1}\right)H\left(t-\frac{3H}{c_1}\right)\delta(x_1,x_2) + \left\{\pi^{-2}\int_{q=0}^{Q_1^{\mathrm{II}}(t)} \mathrm{Im}\left[\mathscr{F}^{\mathrm{II}}_{i,r}(p^{\mathrm{II}}(t,q),q)\left(\frac{\partial p^{\mathrm{II}}}{\partial t}\right)\right] dq\right\}\chi_{[T_1^{\mathrm{II}}(0),T_2^{\mathrm{II}}(0)]}(t)$$
$$+\left\{\pi^{-2}\int_{q=Q_2^{\mathrm{II}}(t)}^{Q_1^{\mathrm{II}}(t)} \mathrm{Im}\left[\mathscr{F}^{\mathrm{II}}_{i,r}(p^{\mathrm{II}}(t,q),q)\left(\frac{\partial p^{\mathrm{II}}}{\partial t}\right)\right] dq\right\}H[t-T_2^{\mathrm{II}}(0)], \tag{77}$$

in which $q=Q_1^{\mathrm{II}}(\tau)$ and $q=Q_2^{\mathrm{II}}(\tau)$ are the (unique) inverses of $\tau=T_1^{\mathrm{II}}(q)$ and $\tau=T_2^{\mathrm{II}}(q)$, respectively. They follow from Eq. (75), which is cubic in q, with the aid of Cardano's formula and are explicitly given in De Hoop and De Hoop.[13] From Eq. (77) it is evident that $T_1^{\mathrm{II}}(0)$ and $T_2^{\mathrm{II}}(0)$ are the arrival times of two wave fronts.

Through the substitutions in accordance with Eq. (A5), the inverse square root singularities at the limits of integration on the right-hand side of Eq. (77) are removed, after which the integrals are evaluated numerically with the aid of the trapezoidal rule.

VI. POLE CONTRIBUTIONS TO THE APPROXIMATED GREEN'S FUNCTIONS

The pole contributions to the approximated Green's functions are evaluated along the lines indicated in Appendix B. From the analysis presented there, it follows that first we have to find the range of the q values for which each pole contributes, with the accompanying region in space where the relevant contribution shows up.

A. The first-order approximation

The first-order approximation to the incident wave Green's function has only a single pole at $p=p_0^{\mathrm{I}}$ as given by Eq. (48). The corresponding vertical travel-time shift is

$$\tau^{\mathrm{I}}_{i;0} = |x_3|\gamma_1^{\mathrm{I}}(p_0^{\mathrm{I}}(q),q) = 0. \tag{78}$$

The value $Q^{\mathrm{I}}_{i;0}$ of q for which the pole and the point of intersection of the modified Cagniard path with the real p axis coincide follows from

$$(Q^{\mathrm{I}}_{i;0})^2 = \left(\frac{r}{|x_3|}\right)^2\frac{1}{c_1^2}-\frac{2}{c_1^2}. \tag{79}$$

Since $(Q^{\mathrm{I}}_{i;0})^2\geqslant 0$ in the region of space where $r/|x_3|\geqslant\sqrt{2}$, the pole contributes in this region. Its contribution is found as

$$G^{\mathrm{I}}_{i;0} = \frac{\rho_1}{2\pi c_1}\frac{1}{[t^2-(T^{\mathrm{I}}_{i;0,1})^2]^{1/2}}\chi_{[T^{\mathrm{I}}_{i;0,1},T^{\mathrm{I}}_{i;0,2}]}(t), \tag{80}$$

in which

$$T^{\mathrm{I}}_{i;0,1} = \sqrt{2}\left(\frac{r}{c_1}\right),\quad T^{\mathrm{I}}_{i;0,2} = \left(\frac{r}{|x_3|}\right)\left(\frac{r}{c_1}\right). \tag{81}$$

The first-order reflected-wave Green's function has simple poles at $p=p_0^{\mathrm{I}}$ as given by Eq. (48) and at $p=p_R^{\mathrm{I}}$ as given by Eq. (50). If $c_1>c_2$, we have $p_0^{\mathrm{I}}<p_R^{\mathrm{I}}$; if $c_1<c_2$, we have $p_0^{\mathrm{I}}>p_R^{\mathrm{I}}$. If $c_1=c_2$ and $\rho_1\neq\rho_2$, there is only a single pole at p_0^{I}, with multiplicity 1. For the first pole the corresponding vertical travel-time shift is

$$\tau^{\mathrm{I}}_{r;0} = (2h-x_3)\gamma_1^{\mathrm{I}}(p_0^{\mathrm{I}}(q),q) = 0 \tag{82}$$

and the value $Q^{\mathrm{I}}_{r;0}$ of q for which the pole and the point of intersection of the modified Cagniard path with the real p axis coincide follows from

$$(Q^{\mathrm{I}}_{r;0})^2 = \left(\frac{r}{2h-x_3}\right)^2\frac{1}{c_1^2}-\frac{2}{c_1^2}. \tag{83}$$

Since $(Q^{\mathrm{I}}_{r;0})^2\geqslant 0$ in the region of space where $r/(2h-x_3)\geqslant\sqrt{2}$, the pole contributes in this region. In view of the fact that at $p=p_0^{\mathrm{I}}$ we have $R=-1$, its contribution directly follows from the contribution to the incident wave as

$$G^{\mathrm{I}}_{r;0} = -\frac{\rho_1}{2\pi c_1}\frac{1}{[t^2-(T^{\mathrm{I}}_{0,1})^2]^{1/2}}\chi_{[T^{\mathrm{I}}_{0,1},T^{\mathrm{I}}_{0,2}]}(t), \tag{84}$$

in which now

$$T^{\mathrm{I}}_{0,1} = \sqrt{2}\left(\frac{r}{c_1}\right),\quad T^{\mathrm{I}}_{0,2} = \left(\frac{r}{2h-x_3}\right)\left(\frac{r}{c_1}\right). \tag{85}$$

For the second pole the vertical travel-time shift is

$$\tau^{\mathrm{I}}_R = (2h-x_3)\gamma_1^{\mathrm{I}}(p_R^{\mathrm{I}}(q),q)$$
$$= (2h-x_3)c_1(c_1^{-2}-\langle c\rangle_{\mathrm{I}}^{-2}) \tag{86}$$

and the value Q^{I}_R of q for which the pole and the point of intersection of the modified Cagniard path with the real p axis coincide follows from

$$(Q^{\mathrm{I}}_R)^2 = \left(\frac{r}{(2h-x_3)c_1}\right)^2-\frac{2}{\langle c\rangle_{\mathrm{I}}^2}. \tag{87}$$

Since $(Q^{\mathrm{I}}_R)^2\geqslant 0$ in the region of space where $r/(2h-x_3)>\sqrt{2}(c_1/\langle c\rangle_{\mathrm{I}})$, the pole contributes in this region. Its contribution is found as

$$G^{\mathrm{I}}_R = \frac{\rho_1}{2\pi c_1}\frac{1}{\langle c\rangle_{\mathrm{I}}^{-2}-c_1^{-2}}\frac{(\rho_2c_2)^{-1}-(\rho_1c_1)^{-1}-[(c_2/\rho_2)-(c_1/\rho_1)]\langle c\rangle_{\mathrm{I}}^{-2}}{(c_2/\rho_2)+(c_1/\rho_1)}$$
$$\times\frac{1}{[(t-\tau^{\mathrm{I}}_R)^2-(T^{\mathrm{I}}_{R,1}-\tau^{\mathrm{I}}_R)^2]^{1/2}}\chi_{[T^{\mathrm{I}}_{R,1},T^{\mathrm{I}}_{R,2}]}(t), \tag{88}$$

in which

$$T^{\mathrm{I}}_{R,1} = \sqrt{2}\left(\frac{r}{\langle c\rangle_1}\right) + \tau^{\mathrm{I}}_R,$$

$$T^{\mathrm{I}}_{R,2} = \left(\frac{r}{2h - x_3}\right)\left(\frac{r}{c_1}\right) + \tau^{\mathrm{I}}_R. \tag{89}$$

B. The second-order approximation

The second-order approximation to the incident wave Green's function has only a single pole at $p = p_0^{\mathrm{II}}$ as given by Eq. (56). The corresponding vertical travel-time shift is

$$\tau^{\mathrm{II}}_{i;0} = |x_3|\gamma_1^{\mathrm{II}}(p_0^{\mathrm{II}}(q),q) = 0. \tag{90}$$

The value $Q^{\mathrm{II}}_{i;0}$ of q for which the pole and the point of intersection of the modified Cagniard path with the real p axis coincide follows from

$$(Q^{\mathrm{II}}_{i;0})^2 = \frac{16}{81}\left(\frac{r}{|x_3|}\right)^2\frac{1}{c_1^2} - \frac{4}{3c_1^2}. \tag{91}$$

Since $(Q^{\mathrm{II}}_{i;0})^2 \geqslant 0$ in the region of space where $r/|x_3| \geqslant \frac{3}{2}\sqrt{3}$, the pole contributes in this region. Its contribution is found as

$$G^{\mathrm{II}}_{i;0} = \frac{2\rho_1}{9\pi c_1}\frac{1}{[t^2 - (T^{\mathrm{II}}_{i;0,1})^2]^{1/2}}\chi_{[T^{\mathrm{II}}_{i;0,1}, T^{\mathrm{II}}_{i;0,2}]}(t), \tag{92}$$

in which

$$T^{\mathrm{II}}_{i;0,1} = \left(\frac{2}{\sqrt{3}}\right)\left(\frac{r}{c_1}\right) \quad \text{and} \quad T^{\mathrm{II}}_{i;0,2} = \left(\frac{4r}{9|x_3|}\right)\left(\frac{r}{c_1}\right). \tag{93}$$

The second-order reflected-wave Green's function has simple poles at $p = p_0^{\mathrm{II}}$ as given by Eq. (56) and at $p = p^{\mathrm{II}}_{R;1}$ and $p = p^{\mathrm{II}}_{R;2}$ as given by Eq. (59). If $c_1 > c_2$, we have $p_0^{\mathrm{II}} < p^{\mathrm{II}}_{R;1} < B(q) < p^{\mathrm{II}}_{R;2}$. If $c_1 < c_2$, we have $p^{\mathrm{II}}_{R;1} < p_0^{\mathrm{II}} < p^{\mathrm{II}}_{R;2} < B(q)$. If $c_1 = c_2$ and $\rho_1 \neq \rho_2$, there is only a single pole at $p_0^{\mathrm{II}}(q)$ of multiplicity 1. For the first pole the corresponding vertical travel-time shift is

$$\tau^{\mathrm{II}}_{r;0} = (2h - x_3)\gamma_1^{\mathrm{II}}(p_0^{\mathrm{II}}(q),q) = 0 \tag{94}$$

and the value $Q^{\mathrm{II}}_{r;0}$ of q for which the pole and the point of intersection of the modified Cagniard path with the real p axis coincide follows from

$$(Q^{\mathrm{II}}_{r;0})^2 = \frac{16}{81}\left(\frac{r}{2h - x_3}\right)^2\frac{1}{c_1^2} - \frac{4}{3c_1^2}. \tag{95}$$

Since $(Q^{\mathrm{II}}_{r;0})^2 \geqslant 0$ in the region of space where $r/(2h - x_3) \geqslant \frac{3}{2}\sqrt{3}$, the pole contributes in this region. In view of the fact that at $p = p_0^{\mathrm{II}}$ we have $R = -1$, its contribution directly follows from the contribution to the incident wave as

$$G^{\mathrm{II}}_{r;0} = -\frac{2\rho_1}{9\pi c_1}\frac{1}{[t^2 - (T^{\mathrm{II}}_{0,1})^2]^{1/2}}\chi_{[T^{\mathrm{II}}_{0,1}, T^{\mathrm{II}}_{0,2}]}(t), \tag{96}$$

in which now

$$T^{\mathrm{II}}_{0,1} = \left(\frac{2}{\sqrt{3}}\right)\left(\frac{r}{c_1}\right), \quad T^{\mathrm{II}}_{0,2} = \left(\frac{4r}{9(2h - x_3)}\right)\left(\frac{r}{c_1}\right). \tag{97}$$

For the pole $p^{\mathrm{II}}_{R;1}$, the vertical travel-time shift is

$$\tau^{\mathrm{II}}_{R;1} = (2h - x_3)\gamma_1^{\mathrm{II}}(p^{\mathrm{II}}_{R;1}(q),q) = (2h - x_3)\frac{3}{c_1}\frac{c_1^{-2} - \langle c\rangle^{-2}_{\mathrm{II};1}}{3c_1^{-2} - \langle c\rangle^{-2}_{\mathrm{II};1}} \tag{98}$$

and the value $Q^{\mathrm{II}}_{R;1}$ of q for which the pole and the point of intersection of the modified Cagniard path with the real p axis coincide follows from

$$(Q^{\mathrm{II}}_{R;1})^2 = \left(\frac{r}{(2h - x_3)c_1}\right)^2\left[\left(\frac{c_1^2}{3\langle c\rangle^2_{\mathrm{II};1}}\right) - 1\right]^4 - \frac{4}{3\langle c\rangle^2_{\mathrm{II};1}}. \tag{99}$$

Since $(Q^{\mathrm{II}}_{R;1})^2 \geqslant 0$ in the region of space where $r/(2h - x_3) > (4c_1^2/3\langle c\rangle^2_{\mathrm{II};1})^{1/2}/(1 - c_1^2/3\langle c\rangle^2_{\mathrm{II};1})^2$, the pole contributes in this region. Its contribution is found as

$$G^{\mathrm{II}}_{R;1} = \frac{\rho_1 c_1}{3\pi}\frac{3c_1^{-2} - \langle c\rangle^{-2}_{\mathrm{II};1}}{\langle c\rangle^{-2}_{\mathrm{II};1} - c_1^{-2}}\left[(\rho_2 c_2)^{-1}[c_2^{-2} - \langle c\rangle^{-2}_{\mathrm{II};1}]\left(c_1^{-2} - \frac{1}{3}\langle c\rangle^{-2}_{\mathrm{II};1}\right) - (\rho_1 c_1)^{-1}[c_1^{-2} - \langle c\rangle^{-2}_{\mathrm{II};1}]\right.$$
$$\left.\times\left(c_2^{-2} - \frac{1}{3}\langle c\rangle^{-2}_{\mathrm{II};1}\right)\right]\{[(\rho_2 c_2)^{-1} + (\rho_1 c_1)^{-1}][\langle c\rangle^{-2}_{\mathrm{II};2} - \langle c\rangle^{-2}_{\mathrm{II};1}]\}^{-1}$$
$$\times\frac{1}{[(t - \tau^{\mathrm{II}}_{R;1})^2 - (T^{\mathrm{II}}_{R;1,1} - \tau^{\mathrm{II}}_{R;1})^2]^{1/2}}\chi_{[T^{\mathrm{II}}_{R;1,1}, T^{\mathrm{II}}_{R;1,2}]}(t), \tag{100}$$

in which

$$T^{\mathrm{II}}_{R;1,1} = \left(\frac{2}{\sqrt{3}}\right)\left(\frac{r}{\langle c\rangle_{\mathrm{II};1}}\right) + \tau^{\mathrm{II}}_{R;1}, \tag{101}$$

$$T^{\mathrm{II}}_{R;1,2} = \left(\frac{r}{2h - x_3}\right)\left[\left(\frac{c_1^2}{3\langle c\rangle^2_{\mathrm{II};1}}\right) - 1\right]^2\left(\frac{r}{c_1}\right) + \tau^{\mathrm{II}}_{R;1}. \tag{102}$$

Upon replacing $\langle c\rangle_{\mathrm{II};1}$ by $\langle c\rangle_{\mathrm{II};2}$ in the factor preceding $\chi_{[T^{\mathrm{II}}_{R;1,1}, T^{\mathrm{II}}_{R;1,2}]}(t)$, the contribution from the pole $p^{\mathrm{II}}_{R;2}$ is found.

VII. THE GREEN'S FUNCTIONS IN THE FIRST- AND SECOND-ORDER RATIONAL PARABOLIC APPROXIMATIONS

By combining the constituents derived in Secs. V and VI, the first- and second-order rational parabolic approximations of the incident- and reflected-wave Green's functions are obtained. The results are summarized below.

A. The first-order approximation (incident wave)

For the first-order approximation to the incident wave the constituents given in Eqs. (71) and (80) lead to

$$G_i^{\mathrm{I}} = G_{i;C}^{\mathrm{I}} + G_{i;0}^{\mathrm{I}}, \tag{103}$$

which can be combined to

$$G_i^{\mathrm{I}} = \begin{cases} \dfrac{\rho_1}{4\pi c_1 [t^2 - (T_{i;0,1}^{\mathrm{I}})^2]^{1/2}} \{2H(t - T_{i;0,1}^{\mathrm{I}}) \\ \quad - H[t - T^{\mathrm{I}}(0)]\}, \quad \text{if} \quad r/|x_3| \geqslant \sqrt{2}, \\ \dfrac{\rho_1}{4\pi c_1 [t^2 - (T_{0,1}^{\mathrm{I}})^2]^{1/2}} H[t - T^{\mathrm{I}}(0)], \\ \quad \text{if} \quad r/|x_3| < \sqrt{2}, \end{cases} \tag{104}$$

where

$$T_{i;0,1}^{\mathrm{I}} = \sqrt{2}\left(\frac{r}{c_1}\right) \tag{105}$$

is the arrival time of the artificial head wave. Upon applying the operator $\mathscr{D}_i$ to this function, it is found that the artificial head wave disappears in the other elements of the Green's tensor.

B. The second-order approximation (incident wave)

For the second-order approximation to the incident wave the constituents given in Eqs. (77) and (92) lead to

$$G_i^{\mathrm{II}} = G_{i;C}^{\mathrm{II}} + G_{i;0}^{\mathrm{II}}. \tag{106}$$

The relevant expression cannot be further simplified. Upon applying the operator $\mathscr{D}_i$ to this function, it is again found that the artificial head wave disappears in the other elements of the Green's tensor.

C. The first-order approximation (reflected wave)

For the first-order approximation to the reflected wave the constituents given in Eqs. (71), (84), and (88) lead to

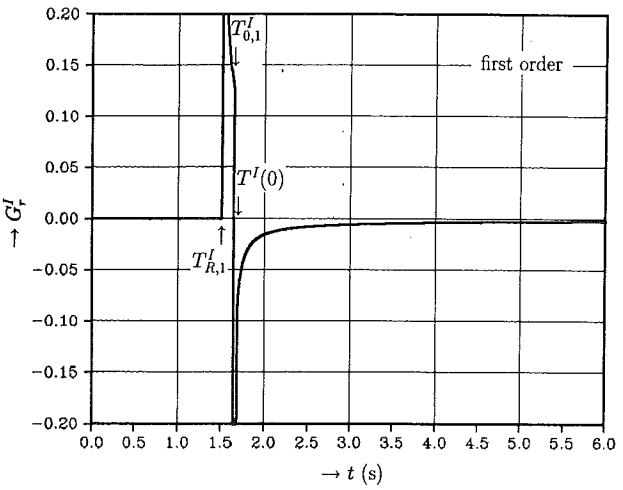

FIG. 9. The first-order approximated reflected-wave Green's function when $r = 1750$ m and $h = 500$ m. The medium parameters are $\rho_1 = \rho_2 = 1000\ \mathrm{kg/m^3}$, $c_1 = 1500$ m/s, and $c_2 = 2828$ m/s.

$$G_r^{\mathrm{I}} = G_{r;C}^{\mathrm{I}} + G_{r;0}^{\mathrm{I}} + G_R^{\mathrm{I}}. \tag{107}$$

The relevant expressions cannot be further simplified. In Figs. 8 and 9, a near and a far horizontal offset trace are shown.

D. The second-order approximation (reflected wave)

For the second-order approximation to the reflected wave the constituents given in Eqs. (77), (96), and (100) lead to

$$G_r^{\mathrm{II}} = G_{r;C}^{\mathrm{II}} + G_{r;0}^{\mathrm{II}} + G_{R;1}^{\mathrm{II}} + G_{R;2}^{\mathrm{II}}. \tag{108}$$

The relevant expressions cannot be further simplified. In Figs. 10–12, a near and a far horizontal offset trace are shown.

To illustrate the near offset results in a typical seismic bandwidth, the Green's functions were also convolved with

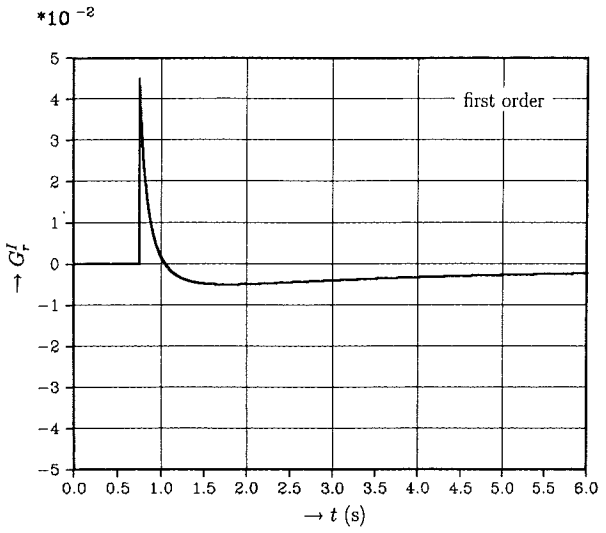

FIG. 8. The first-order approximated reflected-wave Green's function when $r = 500$ m and $h = 500$ m. The medium parameters are $\rho_1 = \rho_2 = 1000\ \mathrm{kg/m^3}$, $c_1 = 1500$ m/s, and $c_2 = 2828$ m/s.

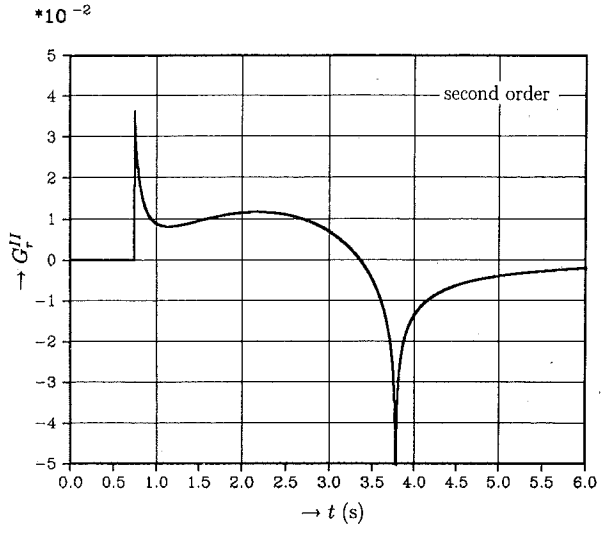

FIG. 10. The second-order approximated reflected-wave Green's function when $r = 500$ m and $h = 500$ m. The medium parameters are $\rho_1 = \rho_2 = 1000\ \mathrm{kg/m^3}$, $c_1 = 1500$ m/s, and $c_2 = 2828$ m/s.

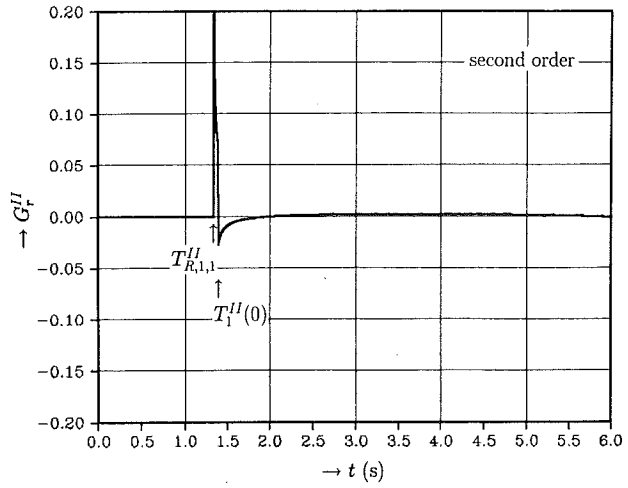

FIG. 11. The second-order approximated reflected-wave Green's function when $r = 1750$ m and $h = 500$ m ($t \leqslant 6s$). The medium parameters are $\rho_1 = \rho_2 = 1000$ kg/m^3, $c_1 = 1500$ m/s, and $c_2 = 2828$ m/s.

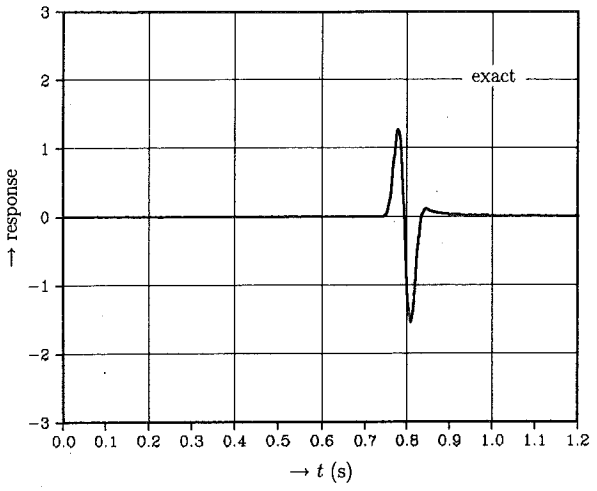

FIG. 13. The Green's function of Fig. 2, after convolution.

the second-order time derivative of a Blackman–Harris window function;[26,27] the results are shown in Figs. 13–15.

VIII. DISCUSSION OF THE RESULTS

For the incident wave, the analysis shows that only for sufficiently "large" horizontal offsets the nonphysical artificial "head waves" do occur. For a restricted source–receiver geometry, the accuracy of the rational parabolic (Thiele) approximations is sufficient, but in a restricted time window only. Further, outside the source plane, the fastest approximate wave will converge toward the physical body wave by increasing the order of approximation though artifacts will remain.

The analysis of the reflected wave shows that the physical head wave cannot be generated in the rational parabolic approximations, while additional nonphysical artifacts are introduced at "large" horizontal offsets. After the convolution of the Green's functions with a source signature (the example of the second-order time derivative of a Blackman–Harris window function is shown), the discrepancies become even more pronounced than the differences in the step discontinuities in the Green's functions at the arrival of the wave would suggest. This means that the inaccuracy of the tail of the Green's function due to the Thiele approximations is certainly observable in a seismic setting in the case of a "shallow" reflecting interface. This effect has been studied by Krail and Brysk.[28] In principle, by applying a Thiele expansion about an oblique direction of propagation, the analysis can be extended to the case of a dipping interface.

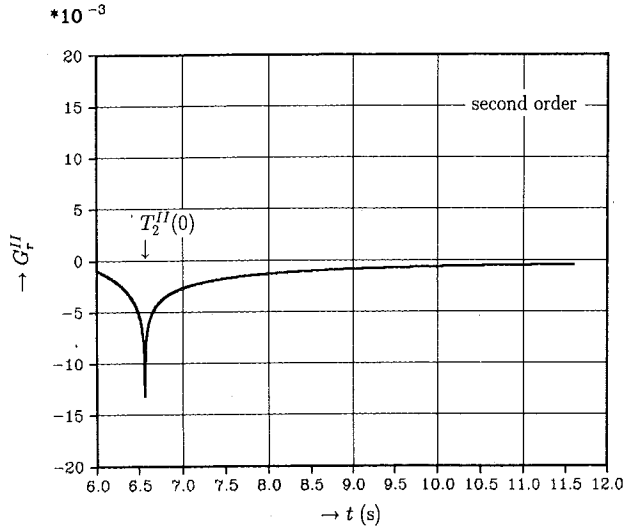

FIG. 12. The second-order approximated reflected-wave Green's function when $r = 1750$ m and $h = 500$ m ($t \geqslant 6s$). The medium parameters are $\rho_1 = \rho_2 = 1000$ kg/m^3, $c_1 = 1500$ m/s, and $c_2 = 2828$ m/s.

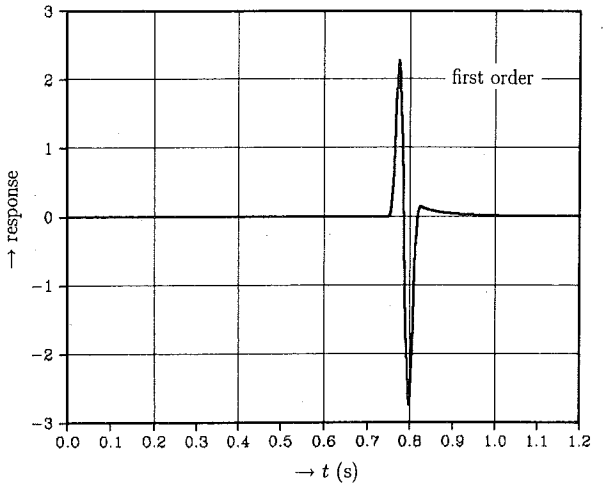

FIG. 14. The Green's function of Fig. 8, after convolution.

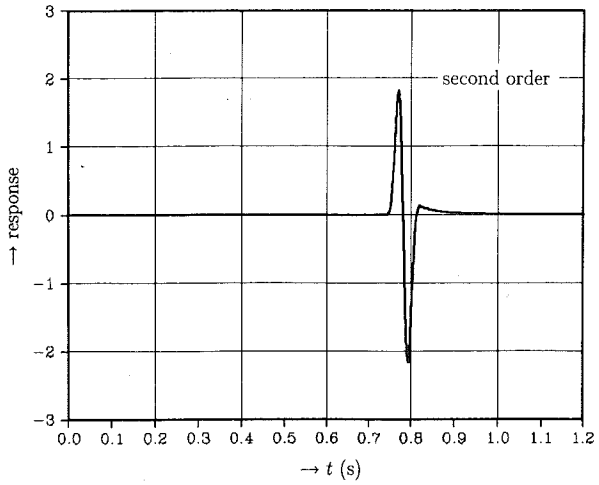

FIG. 15. The Green's function of Fig. 10, after convolution.

APPENDIX A: THE PATH CONTRIBUTION IN THE MODIFIED CAGNIARD METHOD

The path contribution to the wave motion in the half-space $x_3 < h$ is found by solving p from the path equation

$$pr + \gamma_1 H = \tau, \tag{A1}$$

in which γ_1 is, in the exact solution as well as in the rational parabolic approximations, a function of $p^2 - q^2$ and $H = |x_3|$ for the incident wave and $H = 2h - x_3$ for the reflected wave, while τ is to be real and positive (in order to be identifiable as a time delay). Since the expressions in Eq. (A1) are real on (at least part of the) real p axis, they satisfy Schwarz's reflection principle of complex function theory and the resulting path is symmetrical with respect to the real p axis. Since, further, τ is positive, the path is also located in the right half of the complex p plane. This confines the path to the first and fourth quadrants of the p plane. In addition, the transform-domain quantities only depend on q^2. Now, introducing τ as the variable of integration, taking the parts arising from the first and fourth quadrants together, and combining the parts for positive and negative values of q, the inverse transformation Eq. (6) for a typical wave constituent whose transform-domain counterpart is $\tilde{u}$ is obtained as

$$\hat{u}(\mathbf{x},s) = \pi^{-2} \int_{q=0}^{\infty} dq \int_{\tau=T_1(q)}^{T_2(q)} \exp(-s\tau) \times \mathrm{Im}\left[\tilde{u}\left(\frac{\partial p}{\partial \tau}\right)\right] d\tau, \tag{A2}$$

where $\tau = T_1(q)$ and $\tau = T_2(q)$, with $T_1(q) < T_2(q)$, correspond to the begin and end points of the path, respectively. Interchanging the order of integration leads to

$$\hat{u}(\mathbf{x},s) = \int_{\tau=T_1(0)}^{T_2(0)} \exp(-s\tau) d\tau\, \pi^{-2} \times \int_{q=0}^{Q_1(\tau)} \mathrm{Im}\left[\tilde{u}\left(\frac{\partial p}{\partial \tau}\right)\right] dq + \int_{\tau=T_2(0)}^{\infty} \exp(-s\tau) d\tau\, \pi^{-2} \times \int_{q=Q_2(\tau)}^{Q_1(\tau)} \mathrm{Im}\left[\tilde{u}\left(\frac{\partial p}{\partial \tau}\right)\right] dq, \tag{A3}$$

in which $q = Q_1(\tau)$ and $q = Q_2(\tau)$ are the unique inverses of $\tau = T_1(q)$ and $\tau = T_2(q)$, respectively. Applying Lerch's theorem[23] leads to the space-time domain result

$$u(\mathbf{x},t) = \pi^{-2} \int_{q=0}^{Q_1(t)} \mathrm{Im}\left[\tilde{u}\left(\frac{\partial p}{\partial t}\right)\right] dq\, \chi_{[T_1(0),T_2(0)]}(t) + \pi^{-2} \int_{q=Q_2(t)}^{Q_1(t)} \mathrm{Im}\left[\tilde{u}\left(\frac{\partial p}{\partial t}\right)\right] dq \times H[t - T_2(0)], \tag{A4}$$

where $\chi_{[T_1(0),T_2(0)]}(t)$ is the characteristic function of the interval $T_1(0) < t < T_2(0)$, which is defined as the value 1 on the indicated interval and the value 0 outside it.

The integrands in Eq. (A4) can have inverse square-root singularities at the lower and/or upper limits of integration. These are removed by the substitution

$$q^2 = Q_2^2(t)\cos^2(\psi) + Q_1^2(t)\sin^2(\psi), \tag{A5}$$

which changes the interval of integration to $0 < \psi < \pi/2$, after which the integrals are evaluated with the aid of the trapezoidal rule. The corresponding Jacobian is

$$\frac{\partial q}{\partial \psi} = \frac{(Q_2^2 - Q_1^2)\sin(\psi)\cos(\psi)}{[Q_1^2\cos^2(\psi) + Q_2^2\sin^2(\psi)]^{1/2}}. \tag{A6}$$

In some integrals to be encountered in the main text, $Q_2(t) = 0$.

These results are repeatedly used in the main text.

APPENDIX B: THE POLE CONTRIBUTION IN THE MODIFIED CAGNIARD METHOD

A pole contribution to the wave motion results from the residue of the integrand in the complex p plane at that pole. Such poles always arise from zeros in the denominator of expressions that contain as variables only $p^2 - q^2$ in their arguments. Let a zero in this argument be denoted by c_0^{-2} and let the corresponding value of p be given by p_0. Then,

$$p^2 - q^2 = c_0^{-2} \quad \text{or} \quad p_0 = p_0(q) = (q^2 + c_0^{-2})^{1/2} > 0. \tag{B1}$$

In view of this, the pole values of the vertical slownesses γ_1 and γ_2 are independent of q and this property carries over to all transform-domain wave constituents (that contain the excitation coefficient γ_1^{-1} and the reflection coefficient R), since in them the variables p and q only occur through γ_1 and γ_2. Using this in the inverse transformation Eq. (6), the corresponding residue contribution is obtained as

$$\hat{u}_0 = -\frac{1}{2\pi} \int_{q=0}^{Q_0} \exp\{-s[p_0(q)r + \tau_0]\} \times \frac{\{\tilde{u}(p,q)[p^2 - q^2 - c_0^{-2}]\}|_{p=p_0(q)}}{p_0(q)} dq, \tag{B2}$$

in which

$$\tau_0 = \gamma_0 H, \tag{B3}$$

with

$$\gamma_0 = \gamma_1 [p_0(q), q], \tag{B4}$$

can be interpreted as a vertical travel time. In Eq. (B2), we have taken into account that during the contour deformation the departure from the imaginary p axis is to the right and that the pole is, in general, only passed for a finite range $0 < q < Q_0$ of q values, in which Q_0 follows from the condition that the pole coincides with a point of intersection of the modified Cagniard path with the real p axis. These points follow from the contour equation by requiring $\partial_\tau p|_{p=p_0(q)} = 0$, since τ reaches a minimum at such a point of intersection. Replacing the variable of integration q by τ according to

$$p_0(q) r + \tau_0 = \tau, \tag{B5}$$

i.e.,

$$q(\tau) = \left[\left(\frac{\tau - \tau_0}{r} \right)^2 - \frac{1}{c_0^2} \right]^{1/2}, \tag{B6}$$

Eq. (B2) takes the form

$$\hat{u}_0 = -\frac{1}{2\pi} \{ \tilde{u}(p,q) [p^2 - (p_0(q))^2] \}|_{p=p_0(q)} \times \int_{\tau=T_1}^{T_2} \exp(-s\tau) \frac{(\partial q/\partial \tau)}{p_0(q(\tau))} d\tau, \tag{B7}$$

in which

$$T_1 = \tau_0 + (r/c_0) \quad \text{and} \quad T_2 = \tau_0 + r(Q_0^2 + c_0^{-2})^{1/2}. \tag{B8}$$

In view of Lerch's theorem, the corresponding time-domain result is

$$u_0 = -\{ \tilde{u}(p,q) [p^2 - (p_0(q))^2] \}|_{p=p_0(q)} \times \frac{1}{2\pi [(t-\tau_0)^2 - (T_1 - \tau_0)^2]^{1/2}} \chi_{[T_1, T_2]}(t). \tag{B9}$$

This contribution is only present for those positions in space where during the process of contour deformation the pole is passed. The latter condition is equivalent to the requirement $Q_0^2 \geqslant 0$.

This result is repeatedly used in the main text.

[1] C. Brezinski, *The History of Continued Fractions and Padé Approximations* (Springer-Verlag, Berlin, 1991).

[2] V. I. Klyatskin and V. I. Tatarskii, "The parabolic equation approximation for propagation of waves in a medium with random inhomogeneities," Sov. Phys. JETP **31**, 335–339 (1970).

[3] M. A. Guzev and V. I. Klyatskin, "Approximation of the parabolic equation and the wavefield of a point source in a layered random medium," Waves Random Media **1**, 275–286 (1991).

[4] J. F. Claerbout, "Coarse grid calculations of waves in inhomogeneous media with application to delineation of complicated seismic structure," Geophysics **35**, 407–418 (1970).

[5] S. T. McDaniel, "Parabolic approximations for underwater sound propagation," J. Acoust. Soc. Am. **58**, 1178–1185 (1975).

[6] F. D. Tappert, "The parabolic approximation method," in *Wave Propagation in Underwater Acoustics*, Lecture Notes in Physics No. 70 edited by J. B. Keller and J. S. Papadakis (Springer-Verlag, New York, 1977), p. 224–287.

[7] P. G. Kelamis and E. Kjartansson, "Forward modeling in the frequency-space domain," Geophys. Prosp. **33**, 252–262 (1985).

[8] R. R. Greene, "The rational approximation to the acoustic wave equation with bottom interaction," J. Acoust. Soc. Am. **76**, 1764–1773 (1984).

[9] M. W. Lee and S. Y. Suh, "Optimization of one-way wave equations," Geophysics **50**, 1634–1637 (1985).

[10] L. Halpern and L. N. Trefethen, "Wide-angle one-way wave equations," J. Acoust. Soc. Am. **86**, 1397–1404 (1988).

[11] J. A. De Santo, "Relation between the solutions of the Helmholtz and the parabolic equations for sound propagation," J. Acoust. Soc. Am. **62**, 295–297 (1977).

[12] M. D. Collins, "Applications and time-domain solution of higher-order parabolic equations in underwater acoustics," J. Acoust. Soc. Am. **86**, 1097–1102 (1989).

[13] M. V. de Hoop and A. T. de Hoop, "Scalar space-time waves in their spectral domain first- and second-order Thiele approximations," Wave Motion **15**, 229–265 (1992).

[14] P. G. Richards and C. W. Frasier, "Scattering of elastic waves from depth-dependent inhomogeneities," Geophysics **41**, 441–458 (1976).

[15] R. T. Shuey, "A simplification of the Zoeppritz equations," Geophysics **50**, 609–614 (1985).

[16] J. Corones, "Bremmer series that correct parabolic approximations," J. Math. Anal. Appl. **50**, 361–372 (1975).

[17] J. J. McCoy, L. Fishman, and L. N. Frazer, "Reflection and transmission at an interface separating transversely inhomogeneous acoustic half-spaces," Geophys. J.R.A.S. **85**, 543–562 (1986).

[18] L. Hatton, K. Larner, and B. S. Gibson, "Migration of seismic data from inhomogeneous media," Geophysics **46**, 751–767 (1981).

[19] A. T. de Hoop, "A modification of Cagniard's method for solving seismic pulse problems," Appl. Sci. Res. B **8**, 349–356 (1960).

[20] J. D. Achenbach, *Wave Propagation in Elastic Solids* (North-Holland, Amsterdam, 1973), p. 187.

[21] J. Miklowitz, *The Theory of Elastic Waves and Wave Guides* (North-Holland, Amsterdam, 1978), p. 302.

[22] K. Aki and P. G. Richards, *Quantitative Seismology* (Freeman, San Francisco, 1980), p. 224.

[23] D. V. Widder, *The Laplace Transform* (Princeton U.P., Princeton, 1946), p. 63.

[24] A. T. de Hoop and J. H. M. T. van der Hijden, "Generation of acoustic waves by an impulsive point source in a fluid/solid configuration with a plane boundary," J. Acoust. Soc. Am. **75**, 1709–1715 (1984).

[25] N. Jacobson, *Basic Algebra I* (Freeman, San Francisco, 1974).

[26] J. H. M. T. van der Hijden, *Propagation of Transient Elastic Waves in Stratified Anisotropic Media* (North-Holland, Amsterdam, 1987).

[27] F. J. Harris, "On the use of windows for harmonic analysis with the discrete Fourier transform," Proc. IEEE **66**, 51–83 (1978).

[28] P. M. Krail and H. Brysk, "Reflection of spherical seismic waves in elastic layered media," Geophysics **48**, 655–664 (1983).